Journal of Glaciology, Vol. 44, No. 148, 1998

Instruments and Methods

An improved coherent radar depth sounder

S. Gogineni,[1] T. Chuah,[2] C. Allen,[1] K. Jezek,[3] R. K. Moore[1]

[1]Radar Systems and Remote Sensing Laboratory, The University of Kansas, 2291 Irving Hill Road, Lawrence, Kansas 66045-2969, U.S.A.

[2]Silicon Wireless, 2025 Garcia Avenue, Mountain View, California 94043, U.S.A.

[3]Byrd Polar Research Center, The Ohio State University, 108 Scott Hall, 1090 Carmack Road, Columbus, Ohio 43210-1002, U.S.A.

ABSTRACT. The University of Kansas developed a coherent radar depth sounder during the 1980s. This system was originally developed for glacial ice-thickness measurements in the Antarctic. During the field tests in the Antarctic and Greenland, we found the system performance to be less than optimum. The field tests in Greenland were performed in 1993, as a part of the NASA Program for Arctic Climate Assessment (PARCA). We redesigned and rebuilt this system to improve the performance.

The radar uses pulse compression and coherent signal processing to obtain high sensitivity and fine along-track resolution. It operates at a center frequency of 150 MHz with a radio frequency bandwidth of about 17 MHz, which gives a range resolution of about 5 m in ice. We have been operating it from a NASA P-3 aircraft for collecting ice-thickness data in conjunction with laser surface-elevation measurements over the Greenland ice sheet during the last 4 years. We have demonstrated that this radar can measure the thickness of more than 3 km of cold ice and can obtain ice-thickness information over outlet glaciers and ice margins.

In this paper we provide a brief survey of radar sounding of glacial ice, followed by a description of the system and subsystem design and performance. We also show sample results from the field experiments over the Greenland ice sheet and its outlet glaciers.

1. INTRODUCTION

In 1991, NASA began a coordinated program of airborne and spaceborne observations of the Greenland ice sheet. The primary objective of this program is to determine the mass balance of the ice sheet and its impact on global sea level (Krabill and others, 1995b). To assess the mass balance, three primary measurements are required: surface topography, ice thickness and ice velocity. Accurate measurements of surface topography provide an indication of whether the sections of the ice sheet are in mass equilibrium; repeated measurements yield a direct measure of variations in ice-sheet volume (Krabill and others, 1995a). Regional measurements of ice thickness combined with measurements of surface velocity can be used to estimate thinning or thickening rates through application of mass-continuity arguments (Paterson, 1994).

Surface topography is determined to the 10 cm level using an airborne laser operated on the NASA P-3 aircraft. Aircraft navigation is with a global positioning system (GPS). Surface velocity is estimated by repeated GPS measurements of stations fixed on the ice-sheet surface. Ice thickness and the internal structure of the ice sheet are measured using the ice-sounding radar, also on the P-3. The radar also measures the internal structure of the ice sheet and the physical properties of the glacier bed. The latter information is used to help explain the dynamic behavior of the ice sheet and, hence, in developing a hypothesis to explain any detected changes in ice-sheet volume.

In this paper we discuss the design and application of a new and improved ice-sounding radar, the improved coherent Arctic radar depth sounder (ICARDS). The system was designed to be flown in an aircraft or operated from the ice-sheet surface. It has been shown to be effective in acquiring ice-thickness data for ice thicknesses in excess of 3 km for cold ice. Perhaps more important, it has proven very effective for acquiring ice-thickness and internal-structure data on outlet glaciers located around the ice-sheet margin. Because ice wastage occurs through the outlet glaciers and around the margins of the Greenland ice sheet, data from this radar provide new information about processes occurring in the dynamically active ice-sheet perimeter.

2. BACKGROUND

Radio-echo sounding (RES) has been used for the purpose of obtaining thickness measurements of glacial and sheet ice since the early 1960s. The origins of this approach can be traced to 1933 at Admiral Byrd's base, Little America, Antarctica, where the first indication that snow and ice are transparent to high-frequency radio signals was observed. An investigation by U.S. Army researchers, prompted by pilot reports of the *uselessness* of radar altimeters over ice, and suggesting the transparency of polar ice and snow in the VHF and UHF bands, led Waite and others to demonstrate in 1957 that a radar altimeter (the SCR 718 operating at 440 MHz) could measure the thickness and other features of polar glaciers (Waite and Schmidt, 1961; Robin, 1972). This observation resulted in one of the most important technical advances in glaciology, namely, the development and wide application of RES systems.

Following Waite's demonstration, Evans at Cambridge University's Scott Polar Research Institute (SPRI) developed the first of several VHF systems specifically for radio-echo sounding in 1963. Within the next few years several other research groups began developing and using RES systems, including the U.S. Army Electronics Laboratory (USAEL), the British Antarctic Survey, the Arctic and Antarctic Scientific Research Institute in Leningrad, the Geophysical and Polar Research Center at the University of Wisconsin, the U.S. Army Cold Regions Research and Engineering Laboratory, the Canadian Department of Energy, Mines and Resources, the Technical University of Denmark (TUD), Stanford Research Institute, and the Institut Geografii of the U.S.S.R. Academy of Sciences (Evans, 1967; Evans and Smith, 1969; Gudmandsen, 1969; Weber and Andrieux, 1970; Robin, 1975a; Macheret and Zhuravlev, 1982). These systems, all short-pulse-type radar systems with operating frequencies of 30–600 MHz, successfully sounded ice sheets, ice caps and glaciers (both temperate and polar) in both Greenland and Antarctica. Both surface-based and airborne measurements were conducted. Thickness estimates from RES systems agree with those from seismic and gravity-based estimates (Drewry, 1975). Reflections from internal layers have also been observed since the first RES observations, and a variety of sources for these internal reflections have been identified, including layers of liquid water (Bamber, 1987; Davis and others, 1990), layering involving small permittivity changes due to changes in acidity (from large volcanic events) (Millar, 1981), changes in the size or shape of air bubbles within the ice (Ackley and Keliher, 1979), and variations in ice-crystal orientation and density (Harrison, 1973). Layers produced by the small permittivity changes represent isocrones and are useful in the interpretation of climate information (Gudmandsen, 1975; Jacobel and Hodge, 1995). In addition to measurements of ice thickness and layers, other features and characteristics observed include regions of bottom melting and freezing (Neal, 1979), ice-bottom sliding velocity (Doake, 1975), glacier velocity (Doake and others, 1976), sub-ice lakes formed by pressure melting (Oswald, 1975), and bottom crevasses (Jezek and others, 1979). Information on other ice parameters, including signal absorption (Neal, 1976), signal fading patterns (Harrison, 1971; Berry, 1975), propagation velocity (Robin, 1975b) and birefringence (Bentley, 1975; Hargreaves, 1977; Woodruff and Doake, 1979), have been obtained from RES data.

In the next generation of RES systems we see more specialization. For example, to reduce the reflections from nearby walls in sounding valley glaciers, the system frequency is increased to improve system directivity. A 620 MHz system succeeded in sounding Rusty Glacier in Yukon Territory, Canada, where a 35 MHz system and conventional seismic systems had previously been unsuccessful due to echo obscuration by the transmitted radio and seismic pulses and due to the proximity of the valley walls (Clarke and Goodman, 1975). Also, several low-frequency RES systems were developed specifically for sounding temperate glaciers where absorption losses are significant due to higher ice temperatures and the presence of liquid water. Systems with frequencies of 1–32 MHz have been successfully used by numerous researchers to sound temperate glaciers (Strangway and others, 1974; Watts and England, 1976; Björnsson and others, 1977; Sverrisson and others, 1980; Watts and Wright, 1981).

Techniques have also been developed for determining additional information on both the geography and roughness of subglacial terrain. Significant changes in the polarization of the returned echoes from land ice and an ice shelf indicate that tidal strain on crystal orientation at the hinge zone results in a large change in birefringence of the ice, suggesting that polarization could be used to distinguish floating from grounded ice (Woodruff and Doake, 1979). A method for continuously monitoring the returned echo power from a subglacial ice/rock or ice/water interface can detect changes in the reflection coefficient and the absorption properties of the ice, as well as identifying the changing nature of the basal reflection properties along a flowline (Neal, 1976). As part of a physics experiment investigating a theoretical fifth force affecting Newton's inverse square law for gravitation, an extensive series of RES measurements were made around the Dye-3 complex in southern Greenland. Sounding data were collected along 124 radial lines, each about 5 km in length. This produced a map of bedrock topography with an uncertainty of <5 m over most of the survey area (Fisher and others, 1989). A precise grid pattern was flown over the summit region of Greenland with the TUD RES system to obtain both ice-surface and ice-bottom topography to accuracies of ± 6 m and ± 50–125 m, depending on the bottom roughness (Hodge and others, 1990).

As enabling technologies emerged, RES systems became more capable. Digital data acquisition, signal processing and recording significantly improved system capabilities, not the least of which is dynamic range (Goodman, 1975; Sivaprasad, 1978; Wright and others, 1989). Walford and others developed a coherent RES system permitting the measurement of both the amplitude and phase of the received signal (Walford and others, 1977; Walford and Harper, 1981). Synthetic aperture radar (SAR) techniques were applied to RES data by researchers from the British Antarctic Survey to produce two-dimensional maps of echo strength showing the grounding line of a glacier in the Antarctic Peninsula (Musil and Doake, 1987). The coherent Antarctic radar depth sounder (CARDS), the first RES system designed completely with solid-state, computerized components, which is coherent and employs pulse compression to reduce peak transmit power requirements, was field-tested in Antarctica by researchers at the University of Kansas (Raju and others, 1990).

In the 1990s, a new generation of specialized RES systems has emerged to address specific glaciological questions. A miniature impulse RES system capable of operating from 1 to 200 MHz was developed and field-tested by Canadian researchers for sounding glaciers and ice caps (Narod and Clarke, 1994). Researchers from the University of Münster developed and fielded two ground-based 35 MHz RES systems: the first was a single-pulse system intended to measure the reflections from internal layering with high resolution; the second uses a burst transmitter designed to penetrate the sheet ice and observe the underlying bedrock (Hempel and Thyssen, 1993). Norwegian researchers applied SAR techniques to image the internal structure of the subpolar glacier Slakbreen in Spitsbergen, Svalbard, Norway, using range-gated synthetic pulse (stepped frequency modulation) systems operating from 5 to 20 MHz and from 320 to 370 MHz to investigate various geophysical phenomena (Hamran and Aarholt, 1993). Researchers from the University of Alaska at Fairbanks used a 1.7 MHz impulse-type RES system to measure a cross-section of Taku Glacier,

Alaska, and estimate the mass-balance flux (Nolan and others, 1995).

Finally, the value of RES data depends on accurate knowledge of location. Therefore navigation and position-measurement techniques are of great significance to RES systems. When RES systems were first field-tested, navigation relied on observation by system operators, which is significantly hampered in regions without discernible landmarks. In 1967, navigation records, including a galvanometer showing aircraft heading, air temperature, static pressure and airspeed, were recorded along with airborne RES data. By 1971, an inertial navigation system, the Litton 51C, was used to annotate the RES data with position information (Evans and others, 1972; Robin, 1975a). Position-measurement systems employing microwave signals and transponders at known geographic points have been used in ground-based RES experiments within limited areas with an accuracy of $\pm$ 10 m (Goodman, 1975). By the late 1970s, LORAN and satellite navigation were available, providing less accurate yet affordable position information on a global basis suitable for RES applications (Sverrisson and others, 1980). A Doppler navigator linked through a Tactical Air Navigation System navigation computer was used in 1983 to provide a continuous read-out of latitude and longitude with sub-kilometer accuracy (Drewry and Liestøl, 1985; Gorman and Cooper, 1987). Currently, differential GPS data are collected with RES measurements, reducing positional uncertainties to $\pm$ 2–5 m (Nolan and others, 1995).

Table 1 shows an updated summary of the characteristics of the various time-domain radar sets; it was first tabulated by Goodman (1975).

3. SYSTEM DESIGN AND EVALUATION

The system described here is a modified and improved version of the radar system reported by Raju and others (1990). Figure 1 shows the basic elements of the radar system. It operates at a center frequency of 150 MHz with peak transmit power of about 200 W. The transmitter generates a 1.6 μs long pulse using a surface acoustic wave (SAW) expander. This pulse is coupled to the transmit antenna consisting of a four-element dipole array. An identical receive antenna collects the reflected signal. This signal is amplified using a low-noise receiver and compressed using a SAW filter to a pulse about 60 ns wide. A coherent detector generates in-phase (I) and quadrature (Q) signals from the compressed signal. Two identical A/D converters digitize the I and Q signals. These digitized signals are coherently summed, detected and stored on a disk for further processing. Important system parameters are provided in Table 1 (CARDS, U.S.A.).

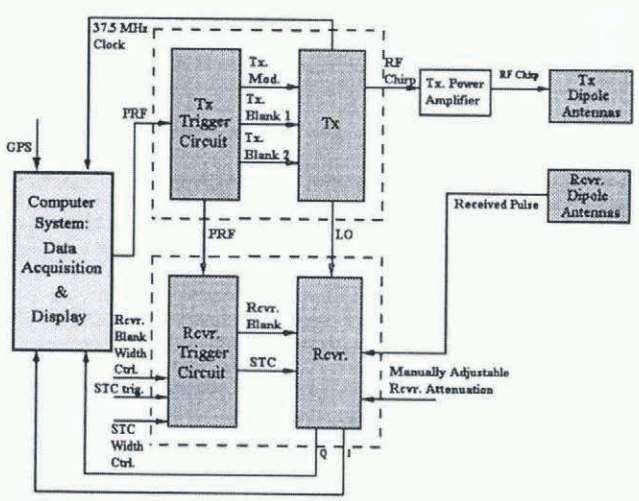

Fig. 1. Block diagram of ICARDS. Blocks shaded at a darker gray level were redesigned and rebuilt. The lightly shaded block was modified for improved performance.

3.1. Transmitter

Figure 2 shows the basic elements of the radar transmitter. A crystal-controlled, low-phase-noise oscillator generates the 150 MHz carrier signal with an output power of 9.5 dBm. This signal is supplied to a four-way power divider to generate: (1) a local-oscillator signal to drive the coherent detector; (2) a clock signal for the A/D converters to digitize received signals; (3) the transmit pulse; and (4) a test signal to monitor oscillator characteristics. The local-oscillator signal from the power divider is buffered with a 10 dB attenuator to minimize reflections, amplified to provide power output of 12 dBm, required to drive the coherent detector, and bandpass-filtered to eliminate spurious signals. To generate the clock signal, a counter divides the 150 MHz signal by four to obtain a 37.5 MHz sine wave that is converted into TTL output using a sine-to-TTL converter (Comlinear Corporation, 1995). The transmit pulse is generated by modulating the 150 MHz signal with a 12 ns pulse (waveform A in Fig. 3) using a fast GaAs single-pole double throw (SPDT) switch. A SAW dispersive filter (expander), buffered with 6 dB attenuators at both input and output ports, generates a chirped pulse that spans the 141.5–158.5 MHz frequency band (waveform B in Fig. 3). This chirped pulse is amplified, limited to eliminate the amplitude modulation, and filtered to reduce harmonic products generated by limiting. The expanded pulse passes through two switches and an amplifier. These switches eliminate side lobes introduced by the SAW expander and turn off transmission during the reception interval (waveforms C and D in Fig. 3). Next a driver amplifier increases the power level to 2 W. An additional switch after the 2 W amplifier ensures that the transmitter leakage power during the off time is insignificant. This signal is then amplified to 200 W and coupled to the transmit antenna. Figure 4 shows the measured transmit waveform. The measurements show that the pulse width is 1.6 μs and that limiting has eliminated any amplitude modulation.

3.2. Receiver

Figure 5 shows the five basic elements of the receiver: (1) front end, (2) sensitivity time control (STC) circuit, (3) driver amplifier, (4) compressor and (5) coherent detector.

The front end consists of a bandpass filter to eliminate spurious signals, and a limiter to protect the receiver from damage by strong signals. A fast GaAs SPDT switch blanks the receiver during the transmission period. The switch is followed by a low-noise amplifier with noise figure of 1.1 dB and gain of 32 dB. The output from the front end is supplied to the STC circuit. Two GaAs voltage-variable attenuators and an amplifier are used to provide the STC. The amplifier between the two attenuators compensates for the attenuators' insertion losses. The STC circuit attenuation is variable between 0 and 35 dB. An operator can adjust the turn-on and decay rate of the STC circuit with two panel-mounted potentiometers.

https://doi.org/10.3189/S0022143000002161 Published online by Cambridge University Press

Table 1. An updated summary of various time-domain radars used in radioglaciology

System	*Freq.*	*Peak power*	*Bandwidth*	*Pulse width*	*Range accuracy*[1]	*System perf.*[2,3]	*Ant. gain*	*Beamwidth*	*Dynam. range*[4]	*Source*
	MHz	W	MHz	ns	m	dB	dB	°	dB	
(Australia)	100	5000	10	300	7	175	11			Morgan and Budd (1975)
DENV (Canada)	620	3000	10/30	70/500	2.5/7	154/159	15	5.2	90	Goodman (1970, 1975); Goodman and others (1975)
University of BC (Canada)	840	4100	40	50	4	124	31	18 × 44	80	Narod and Clarke (1980)
TUD (Denmark)	30	1600	1/14	60/1000	5/60	168/180	28	20	70	Gudmandsen (1970, 1975)
TUD (Denmark)	60	10 000/1600/ 1000	14/4/1	1000/500/ 250/125/60	5/25	205/218		22 × 110		Gudmandsen (1977); Hodge and others (1990)
TUD (Denmark)	300			60						Drewry and Meldrum (1978)
SPRI Mark I (England)	35		14	300		127				Walford (1964)
SPRI Mark II (England)	35/50	500–800	14	240	10	160	10			Evans and Smith (1969); Jezek and others (1979); Jezek (1985)
SPRI Mark III (England)	150	300	30	100	2.5	150	13	20	70	Evans (1970)
SPRI Mark IV (England)	35/60	300/1500	14/15	250/350 1000	5	160	8/18	12/90	35/60	Evans and Smith (1969); Doake and others (1976); Gorman and Cooper (1987)
Mark I (Iceland)	2–5	8000	3	800	20	150	−10			Sverrisson and others (1980)
Mark II (Iceland)	2–10	1250/8000	3	100/200	8	150	−10			Björnsson and others (1977); Sverrisson and others (1980)
(Norway)	205	40	14	200	5	120	11	16		Personal communication from G. Østrem, 1970, in Goodman (1975)
SCR-718 (U.S.A.)	440	7	3	500	20	128	4	50	10	Sinsheimer (1947); Weber and Andrieux (1970)
USAEL (U.S.A.)	30	200–400	3	500	20	150	25	30		Rinker and Mock (1967)
ADCOLE (U.S.A.)	600	10	450	1	0.015	90	14	30		Evans (1967); Rinker (unpublished)
ANARE (U.S.A.)	100	5000	10	300	7	173	11	32	10	Evans (1970)
USGS (U.S.A.)	1–15	400–4000	10	1000–66	50			90		Watts and others (1975); Watts and Wright (1981)
CARDS (U.S.A.)	150	200	17	1600	5	190	21	18		Raju and others (1990)
University of Alaska (U.S.A.)	1.7				5					Nolan and others (1995)
1M4 (U.S.S.R.)	213	50 000– 80 000	1	2500	60	180	14	30		Fedorov (1967)
RV-10, -17 (U.S.S.R.)	440	7	6	500		130	2	100		Dowdeswell and others (1984); Kotlyakov and Macheret (1987)
RLS-620 (U.S.S.R.)	620	820	15	100–1000		146–185	19.5	18		Dowdeswell and others (1984); Kotlyakov and Macheret (1987)

[1] Range accuracy refers to resolution in ice ($n = 1.78$).
[2] System performance is total difference between transmitted power and receiver sensitivity.
[3] System performance includes antenna gain.

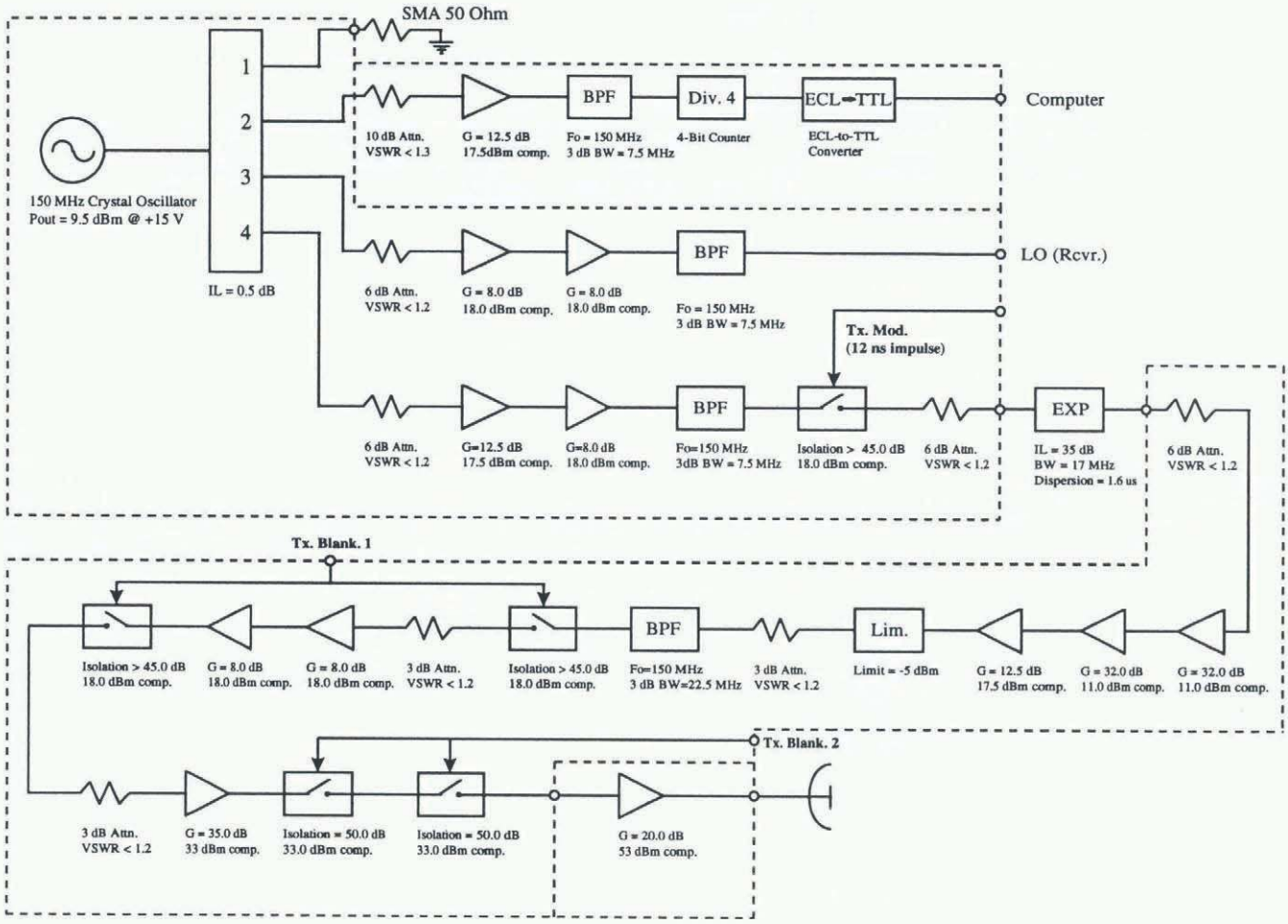

Fig. 2. Block diagram of the radio frequency (RF) section of the ICARDS transmitter. Every block is enclosed as a module in a metal case.

The output from the STC circuit passes to the driver amplifier section that contains a bandpass filter, two 32 dB gain amplifiers and a step attenuator. The filter eliminates any spurious signals introduced by the STC circuit. The step attenuator can be adjusted to provide attenuation between 0 and 63 dB. The two amplifiers and attenuator provide a variable-gain driver amplifier. Using front panel controls, the driver amplifier gain can be set between 0 and 63 dB. The driver amplifier output goes to the compressor section that consists of the SAW compressor with a 37 dB loss and a post-amplifier with a gain of 45 dB to compensate for the SAW device insertion loss. The compressor output goes to the coherent detector that consists of I and Q detectors, amplifiers and low-pass filters. The amplifiers are used to obtain conversion gain of 10 dB from the I and Q detector sections. The low-pass filters, with cut-off frequencies of 9.375 MHz, eliminate aliasing introduced by digitization. The total maximum receiver gain, with minimal STC attenuation and step attenuator setting, is about 100 dB. The radar is normally operated with a gain of 87 dB when STC is at its minimum attenuation setting.

3.3. Timing and control

Radar timing and control signals are derived from the

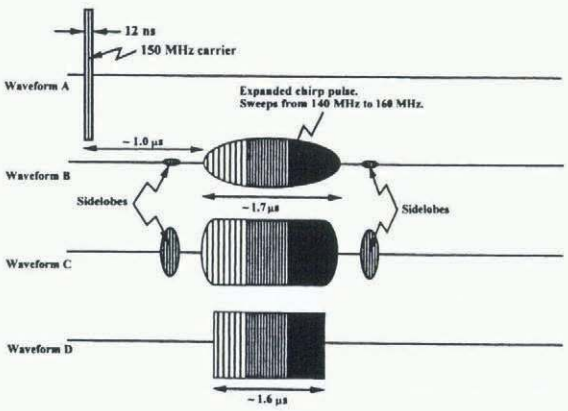

Fig. 3. Transmitter waveform generation process.

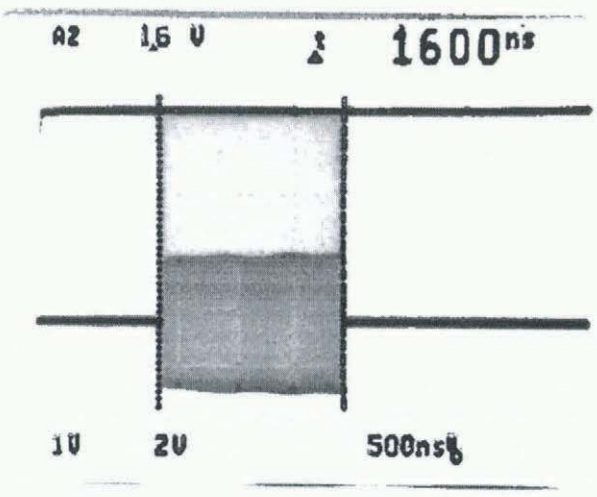

Fig. 4. Oscilloscope display of the RF-chirp waveform, showing a clean 1.6 μs pulse width with no amplitude modulation.

https://doi.org/10.3189/S0022143000002161 Published online by Cambridge University Press

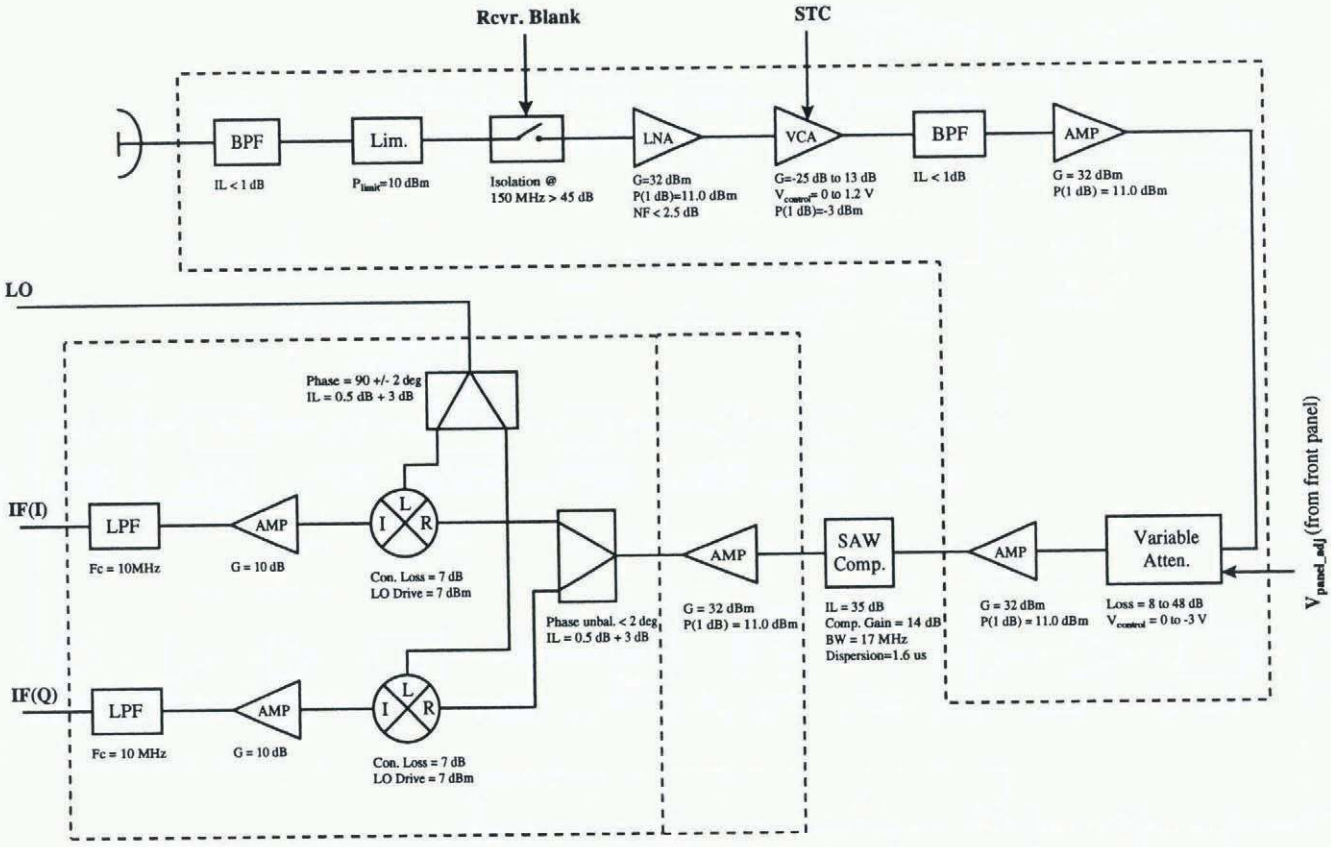

Fig. 5. Block diagram of the RF section of the receiver.

pulse-repetition frequency (PRF) signal. This is generated from the 37.5 MHz TTL signal using a programmable divider. The divider can be programmed to provide any one of the four discrete frequencies: 1100, 2300, 4600 and 9200 Hz.

We use a digital delay generator (Analog Devices Inc., 1996) to obtain a short pulse for modulating the carrier signal. Figure 6a shows this circuit along with the waveforms. The PRF signal from the hex inverter (not shown) is supplied to the trigger input of the delay generator, and the delayed output is applied to the reset input to produce a narrow output pulse. The width of the output pulse is determined by the reset propagation delay, which is typically about 12 ns. The eight-bit digital word that determines the delay is set to provide minimum delay of the leading edge of the output pulse with respect to the trigger signal.

Figure 6b shows the circuit diagram for generating the transmitter blanking signal and corresponding waveforms. We use an integrated circuit (LS221) consisting of a dual monostable multivibrator with positive-transition or negative-transition trigger inputs. A negative-transition trigger input, derived from the hex inverter (not shown), triggers the multivibrator to generate an output pulse whose width is determined by R1 and C1 and can be adjusted by varying R1. This output pulse goes to the negative-transition input of the second multivibrator. During the negative transition time the monostable multivibrator is triggered to generate the blanking pulse. The width of the blanking pulse is determined by R2 and C2, and it can be adjusted using R2. In this configuration the first multivibrator controls the start time, and the second multivibrator controls the duration of the blanking signal. While the output pulse width of the LS221 can be varied from a minimum of 35 ns to a maximum of 7 s, in our configuration the blanking-pulse width range can be varied from 700 ns to 4.2 μs, and the start time of the blanking pulse can be varied from 460 ns to 2.77 μs.

3.4. Digital system

Figure 7 shows the basic elements of the digital system. It consists of: (1) the control circuit to generate PRF and clock signals; (2) two A/D converters to digitize the I and Q signals from the radar receiver; (3) two hard-wired adders to perform coherent integrations; and (4) a digital signal processor to communicate with a host PC and perform both coherent and incoherent integrations.

Two identical eight-bit A/D converters digitize the analog signals at a sampling rate of 18.375 MHz. The hard-wired adders coherently sum the digitized signals and are designed to perform a maximum of 256 additions. A digital signal processor, using an AD-2100 (Analog Devices Inc., 1987), performs coherent additions beyond 256 and incoherent integration. It also generates interrupt signals for data processing and communication with the PC. The control circuit generates a multiphase clock for generating the PRF signal and for defining the data-acquisition window. These signals are generated from the 37.5 MHz signal derived from the coherent oscillator (Xin, 1989).

A standard Pentium-based PC equipped with a 2-GB hard drive and an interface card to control the data acquisition and processor subsystem controls radar operation, stores data and displays data in real time.

3.5. Antennas

The antenna assembly consists of two four-element dipole arrays, one for receive and the other for transmit. The transmit antenna is mounted under the port (left) wing, and the receive antenna under the starboard (right) wing of the P-3 aircraft. Each dipole is constructed with two hollow pipes of 1 in (2.54 cm) diameter and length slightly less than a quarter-wavelength. All four elements are connected to a power

https://doi.org/10.3189/S0022143000002161 Published online by Cambridge University Press

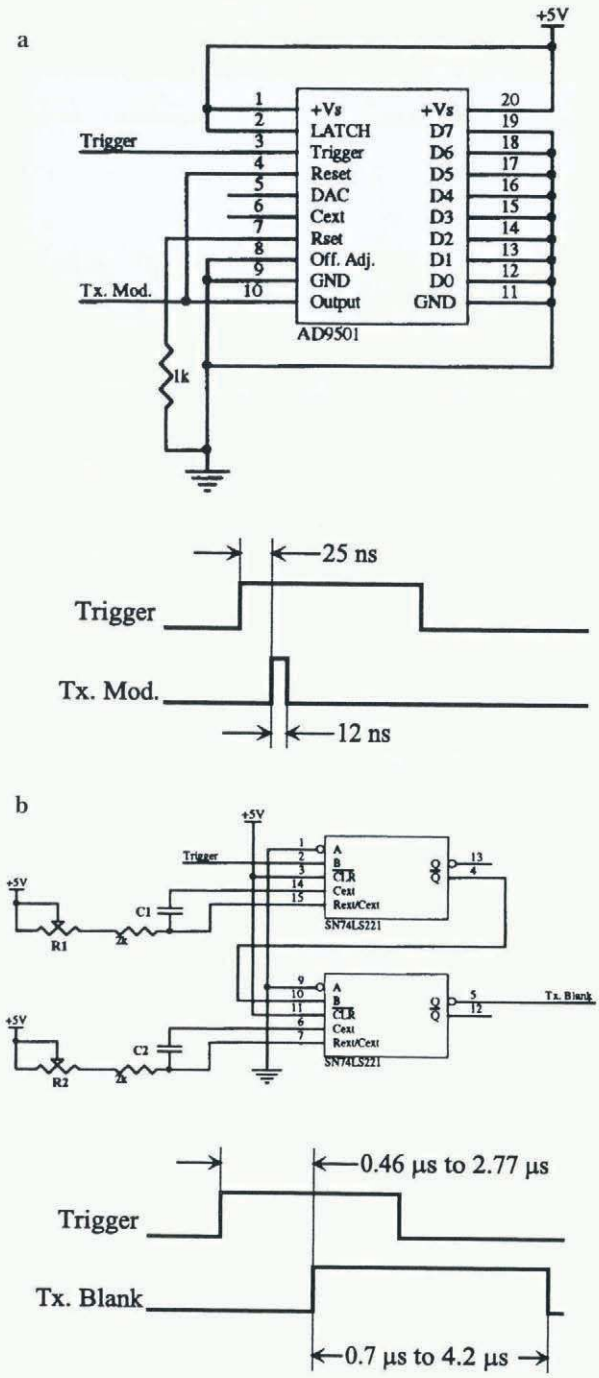

Fig. 6. Circuit and timing diagrams for the transmitter modulator (a) and blanking-signal generator (b).

divider mounted near the antenna assembly, using equal-length 5 m long cables. The transmit pulse is supplied to the power divider input through 20 m long cables. The total of insertion loss in both cables and the power-divider loss is about 3.5 dB. Figure 8 shows a photograph of the transmit antenna mounted under the wing of the P-3 aircraft. The total computed two-way gain of the antenna, including focusing gain for 3 km ice, is about 27 dB (West and Demarest, 1987). The wings of the P-3 aircraft tilt upward by about 7°, which results in an antenna-gain reduction at nadir of about 6 dB.

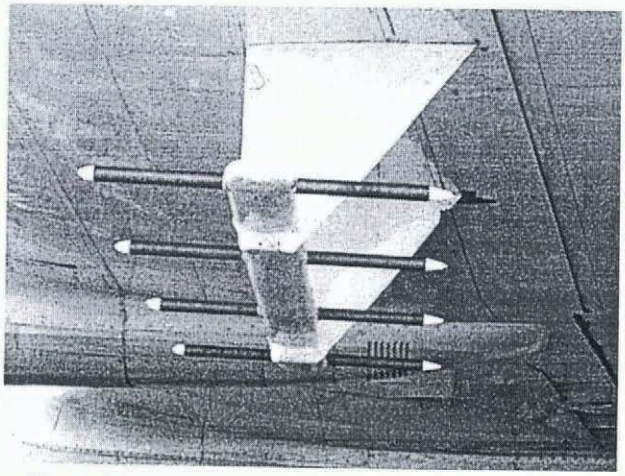

Fig. 8. Transmit antenna mounted under the wing of the N426NA (NASA P3-B) aircraft.

4. SYSTEM EVALUATION

We evaluated the system performance by measuring its noise characteristics and impulse response. Receiver gain must be set such that noise from the coherent detector is higher than the quantization noise of the A/D converter by a factor equal to the signal-processing gain. This gain is the result of coherent and incoherent integrations. Typically we operate the system to obtain a signal-processing gain of about 30 dB, which can be achieved with various combinations of coherent and incoherent integrations. Normally we use coherent integration factors of 128 or 256.

To measure the noise performance, we terminated the receiver input with a 50 Ω load, set the receiver gain at about 87 dB, which is the typical operating gain, and digitized the I and Q signals. Figure 9 shows the results of this test. Between samples 50 and 900 the output noise is reduced to about one A/D count after 1024 coherent integrations. The return below sample No. 50 is caused by transi-

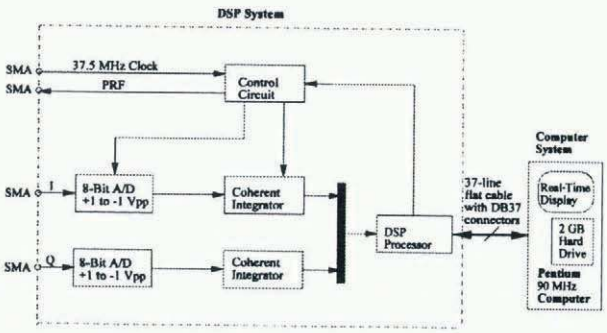

Fig. 7. Block diagram of the digital system.

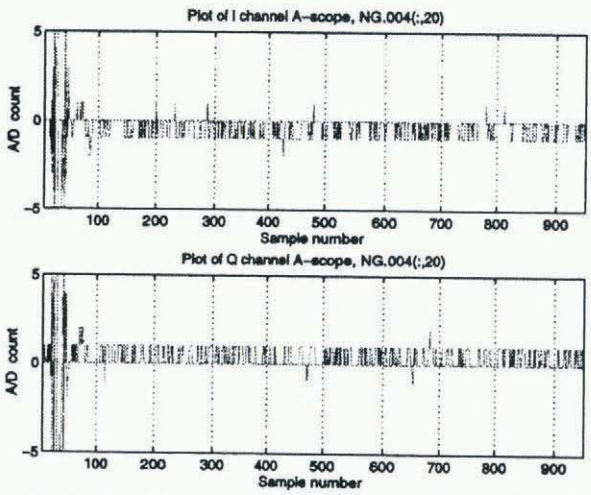

Fig. 9. Test results with receiver input terminated with 50 Ω load and the receiver gain set at about 87 dB.

https://doi.org/10.3189/S0022143000002161 Published online by Cambridge University Press

ents introduced by the receiver-blanking switch. During normal operation over glacial ice this part of the waveform is not digitized, because the start time for digitization is set at a much later time.

We installed the radar on a NASA P-3 aircraft and flew over a relatively calm ocean off the coast near Wallops Island, Virginia, to measure the impulse response and system sensitivity. We set the end of the receiver-blanking interval and the beginning of the STC interval to about 1 μs. We also set the STC circuit to increase the receiver gain to its maximum value immediately after 1 μs. A variable attenuator was inserted between the receive antenna and receiver input. The aircraft flew at an altitude of about 15 000 ft (4500 m) to simulate free-space loss associated with a range of about 3.5 km. The variable attenuator was set to provide an insertion loss of 93 dB. Figure 10 shows the measured impulse response, along with an expanded view of the signal to illustrate the side lobes and the noise performance. The echoes before sample No. 100 are internal feed-through signals. The echo at about sample No. 690 is from the ocean surface. The signal-to-noise ratio is about 16 dB. The total attenuation to reduce the ocean echo to make it 6 dB higher than system noise is about 103 dB. If we assume that the reflection coefficient at the water–ice interface is about 20 dB higher than that for the ice–bedrock interface, the scattering and absorption losses in ice that this system can overcome are about 83 dB.

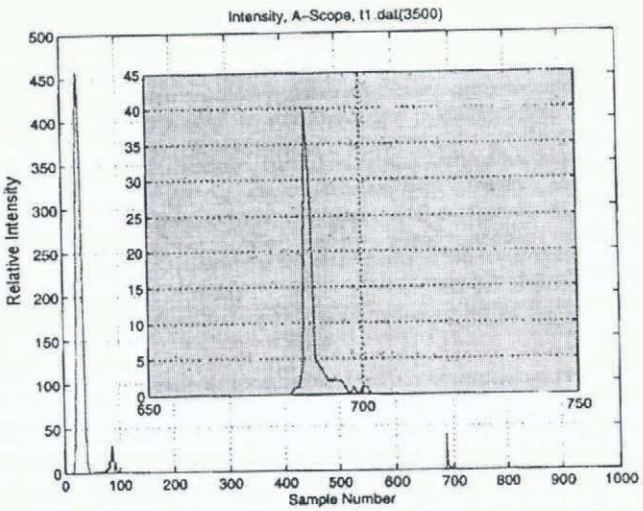

Fig. 10. The measured impulse response along with an expanded view of the signal to illustrate side lobes and noise performance during an airborne flight test.

4.1. Experimental results

Since 1993, we have collected a large volume of data on ice thickness as part of the NASA Program for Arctic Climate Assessment (PARCA). Reports providing first-order results with radio echogram for each flight-line, along with the ice thicknesses derived from these echograms, are available elsewhere (Chuah and others, 1996a, b; Legarsky and others, 1997); here we provide a few sample results to demonstrate radar performance.

Figure 11a shows radar data collected along a flight-line passing within 2.6 km of the deep ice-core drill site in northern Greenland (Dahl-Jensen and others, 1997). The relatively flat bottom topography contributes to the smooth

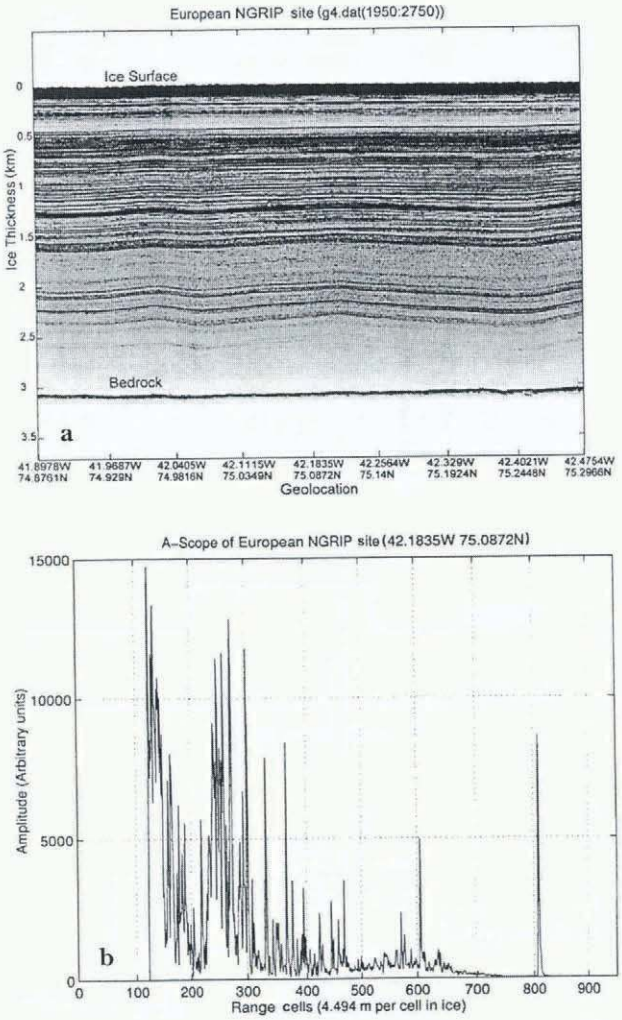

Fig. 11. Radio echogram (a) and an A-scope presentation of signal amplitude vs depth for one sample from the echogram (b) for radar data collected along a flight-line near the deep ice-core drill site in northern Greenland.

internal layers observed to depths greater than 2.6 km throughout the ice column. Echoes near the surface consist of reflections from dielectric discontinuities in the ice. The very flat echoes are multiple reflections between the aircraft and the surface.

Figure 11b shows the amplitude of one sample echo waveform as a function of depth. Near-surface echoes are weak because the STC circuit was set to prevent receiver saturation from the strong primary and multiple echoes of the surface. The STC receiver gain is increased from its minimum value at about zero range to its maximum value for ranges greater than about 1 km. The ice-bottom return occurs at approximately range cell 810 and has a signal-to-noise ratio of about 26 dB. This demonstrates the radar is capable of measuring thicknesses greater than 3 km for cold ice.

Figure 12 shows radar data collected over the southern Greenland ice sheet during the 1997 field season. From the figure we can see several layers both near the surface and at depths of 1 km and beyond. The variation in intensity between the surface and about 400 m depth is due to the blanking switch that protects the receiver from the strong surface echo. We also see significant variation in the bedrock elevation underlying the ice sheet; however, beyond about 1.8–2 km the attenuation exceeds the sensitivity of the radar, and the bottom echo is lost. Many other interesting features

https://doi.org/10.3189/S0022143000002161 Published online by Cambridge University Press

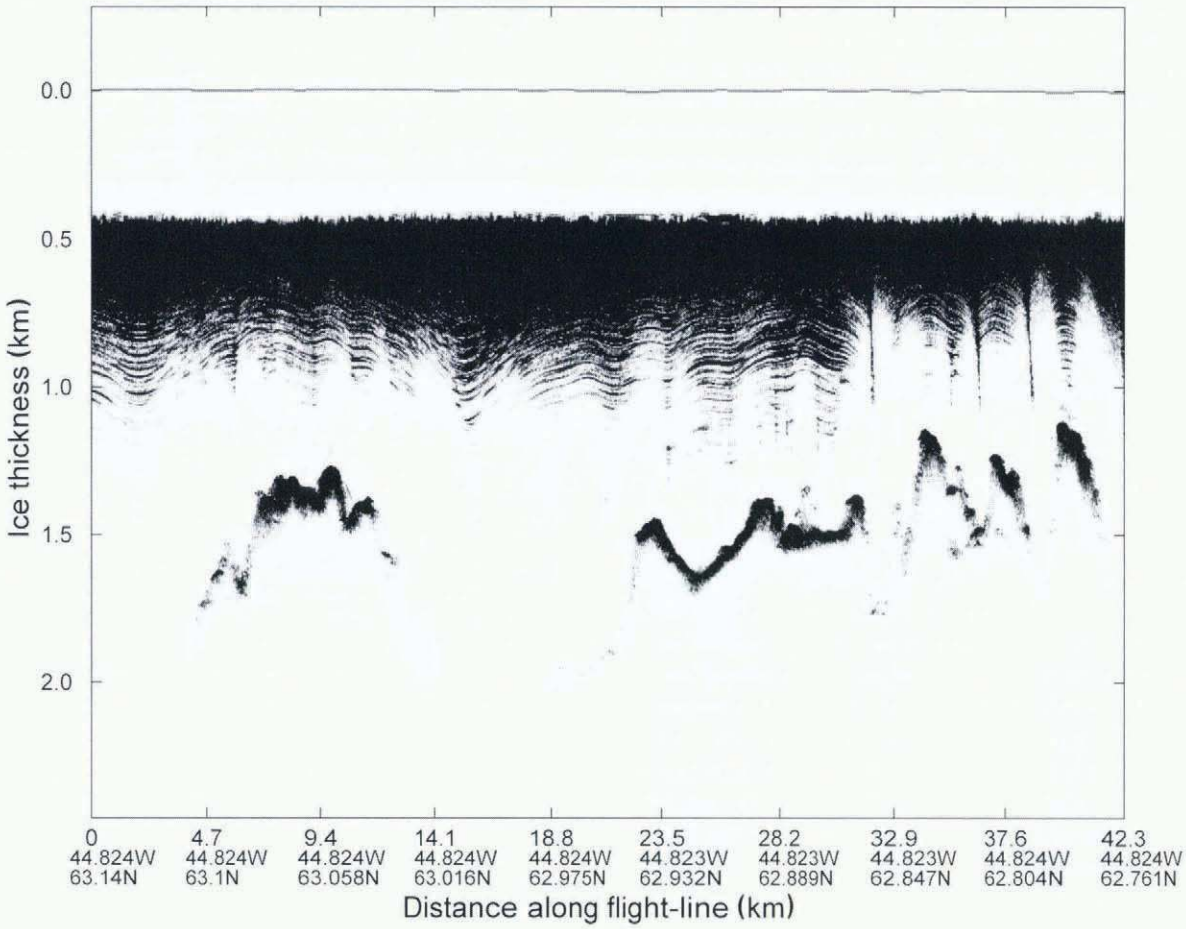

Fig. 12. Radio echogram data collected over the southern Greenland ice sheet during 1997 field season.

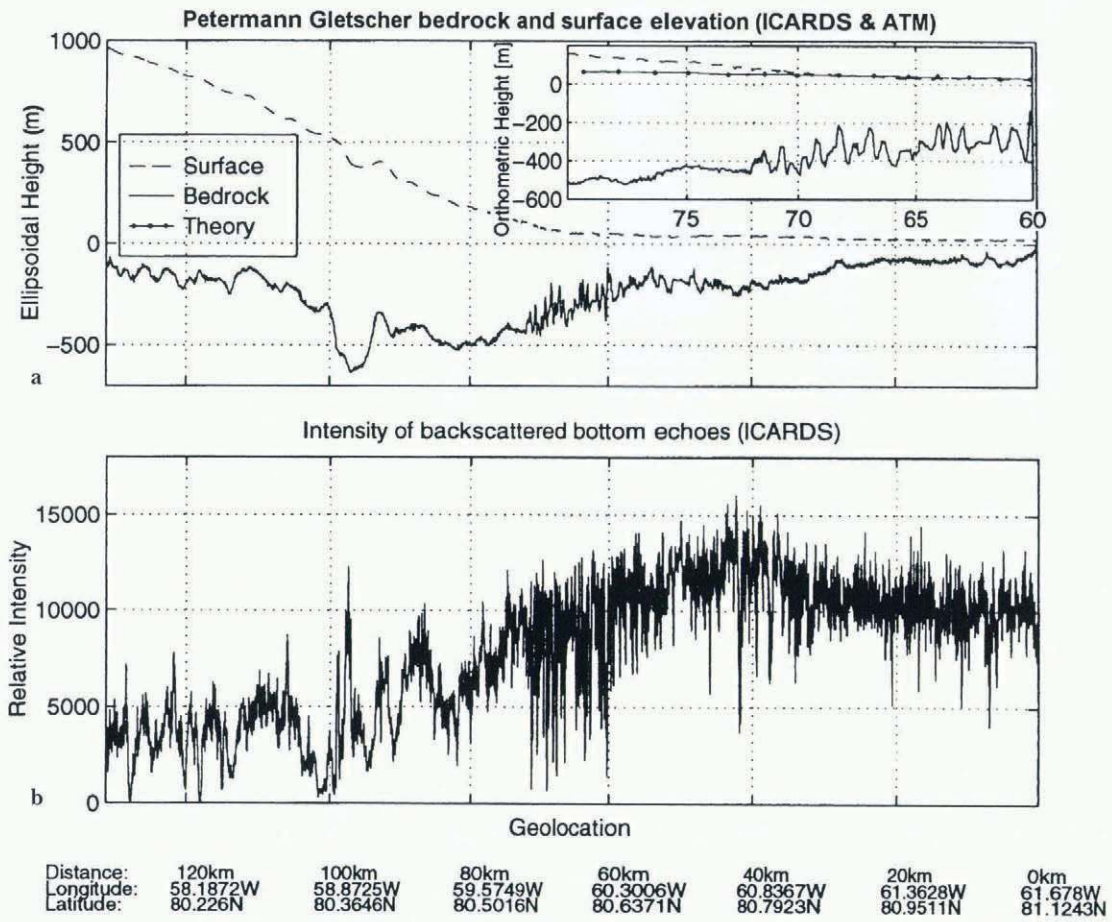

Fig. 13. Radio echogram plot (a) and radar echo intensity (b) showing the surface and bedrock topography along Petermann Gletscher. Inset in (a) illustrates the surface-elevation estimate based on isostatically compensated ice thicknesses.

https://doi.org/10.3189/S0022143000002161 Published online by Cambridge University Press

appear in this image that are not present in the less complex area in northern Greenland. We see this in southern Greenland because the ice temperature is higher than in northern and central Greenland and consequently the absorptive loss is increased. We are exploring techniques to improve the radar sensitivity in order to increase our penetration depth in these regions.

Figure 13 shows surface and basal topography (top) and radar-echo intensity (bottom) along Petermann Gletscher in northwest Greenland. The calving front is located on the rightmost edge of the figure where the ice thickness is only about 60 m. The ice thickness 125 km upstream of the calving margin is over 1100 m and the glacier rests on bedrock about 100 m below sea level. Moving seaward, the ice sheet thins and the bedrock elevation becomes increasingly negative. A sharp increase in echo intensity is associated with a deep trough located about 95 km upstream of the calving margin. We believe this may signify the presence of a small subglacial lake. The echo intensity begins to increase systematically about 80 km from the calving margin. We believe this represents a transition in basal properties as the grounding line of the glacier is approached. Based on echo strength, the location of bottom crevasses and a comparison of surface elevation, with the surface-elevation estimate based on isostatically compensated ice thicknesses (see Fig. 13a, inset), we find that the grounding line occurs about 70 km upstream of the calving margin and near the location determined using interferometric spaceborne SAR techniques (Rignot, 1996).

5. CONCLUSIONS

We redesigned and rebuilt the University of Kansas radar depth sounder to make it fully functional. The system obtains high sensitivity for measuring ice thickness through signal processing and pulse compression. Results show that it provides excellent ice-thickness information over the cold ice, ice margins and outlet glaciers. We plan to collect additional ice-thickness data over the Greenland ice sheet during 1998 and 1999 to augment and supplement existing data. The radar is designed to display radar echograms for the operators in real time. The system is ready for routine data collection.

We plan further improvements to system performance by steering the antenna beam to eliminate gain reduction caused by the slanted wings. We also are developing a new digital signal processing system to incorporate 12-bit A/D converters to increase dynamic range and store data in a coherent mode for implementing more coherent processing.

REFERENCES

Ackley, S. F. and T. E. Keliher. 1979. Ice sheet internal radio-echo reflections and associated physical property changes with depth. *J. Geophys. Res.*, **84**(B10), 5675–5680.

Analog Devices Inc. 1987. *ADSP-2100 applications handbook. Vol. 1.* Norwood, MA, Analog Devices Inc.

Analog Devices Inc. 1996. *Designer's reference manual.* Norwood, MA, Analog Devices Inc.

Bamber, J. L. 1987. Internal reflecting horizons in Spitsbergen glaciers. *Ann. Glaciol.*, **9**, 5–10.

Bentley, C. R. 1975. Advances in geophysical exploration of ice sheets and glaciers. *J. Glaciol.*, **15**(73), 113–135.

Berry, M.V. 1975. Theory of radio echoes from glacier beds. *J. Glaciol.*, **15**(73), 65–74.

Björnsson, H., R. L. Ferrari, K. J. Miller and G. Owen. 1977. A 1976 radio echo sounding expedition to the Vatnajökull ice cap, Iceland. *Polar Rec.*, **18**(115), 375–377.

Chuah, T. S., S. P. Gogineni, C. Allen and B. Wohletz. 1996a. *Radar thickness measurements over the northern part of the Greenland ice sheet.* Lawrence, KS, University of Kansas Center for Research Inc. Radar Systems and Remote Sensing Laboratory. (Technical Report 10470-3.)

Chuah, T. S., S. P. Gogineni, C. Allen and B. Wohletz. 1996b. *Radar thickness measurements over the southern part of the Greenland ice sheet.* Lawrence, KS, University of Kansas Center for Research Inc. Radar Systems and Remote Sensing Laboratory. (Technical Report 10470-2.)

Clarke, G. K. C. and R. H. Goodman. 1975. Radio echo soundings and ice-temperature measurements in a surge-type glacier. *J. Glaciol.*, **14**(70), 71–78.

Comnlinear Corporation. 1995. *Linear databook.* Fort Collins, CO, Comnlinear Corporation.

Dahl-Jensen, D. *and 9 others.* 1997. A search in north Greenland for a new ice-core drill site. *J. Glaciol.*, **43**(144), 300–306.

Davis, C. H., R. H. Dean and W. Xin. 1990. Radar reflections from water injected into an Antarctic glacier. *IEEE Trans. Geosci. Remote Sensing*, **GE-28**(4), 723–726.

Doake, C. S. M. 1975. Glacier sliding measured by a radio-echo technique. *J. Glaciol.*, **15**(73), 89–93.

Doake, C. S. M., M. Gorman and W. S. B. Paterson. 1976. A further comparison of glacier velocities measured by radio-echo and survey methods. *J. Glaciol.*, **17**(75), 35–38.

Dowdeswell, J. A., D. J. Drewry, O. Liestøl and O. Orheim. 1984. Radio echo-sounding of Spitsbergen glaciers: problems in the interpretation of layer and bottom returns. *J. Glaciol.*, **30**(104), 16–21.

Drewry, D. J. 1975. Comparison of electromagnetic and seismic–gravity ice thickness measurements in East Antarctica. *J. Glaciol.*, **15**(73), 137–150.

Drewry, D. J. and O. Liestol. 1985. Glaciological investigations of surging ice caps in Nordaustlandet. *Polar Rec.*, **22**(139), 359–378.

Drewry, D. J. and D. T. Meldrum. 1978. Antarctic airborne radio echo sounding, 1977–78. *Polar Rec.*, **19**(120), 267–273.

Evans, S. 1967. Progress report on radio echo soundings. *Polar Rec.*, **13**(85), 413–420.

Evans, S. 1970. Review of radio echo system performances. *In* Gudmandsen, P. E., *ed. Proceedings of the International Meeting on Radioglaciology, May 1970, Lyngby, Denmark.* Lyngby, Technical University of Denmark. Laboratory of Electromagnetic Theory, 100–102.

Evans, S. and B. M. E. Smith. 1969. A radio echo equipment for depth sounding in polar ice sheets. *J. Phys. E, Ser. 2*, **2**, 131–136.

Evans, S., D. J. Drewry and G. de Q. Robin. 1972. Radio-echo sounding in Antarctica, 1971–72. *Polar Rec.*, **16**(101), 207–212.

Fedorov, B. A. 1967. Primeneniye aktivnoy radiolokatsii dlya izucheniya antarkticheskikh lednikov [Radar sounding of Antarctic ice]. *Inf. Byull. Sov. Antarkt. Eksped.* 62, 19–24.

Fisher, E. *and 6 others.* 1989. Determination of bedrock topography beneath the Greenland ice sheet by three-dimensional imaging of radar sounding data. *J. Geophys. Res.*, **94**(B3), 2874–2882.

Goodman, R. H. 1970. A data collection system for glacier studies. *In Ninth Annual Hydrographic Conference, 27–29 January 1970, Talisman Motor Inn, Ottawa. Proceedings.* Ottawa, Ont., Canadian Hydrographic Service, 69–78.

Goodman, R. H. 1975. Radio echo sounding on temperate glaciers. *J. Glaciol.*, **14**(70), 57–69.

Goodman, R. H., G. K. C. Clarke, G. T. Jarvis, S. G. Collins and R. Metcalfe. 1975. Radio soundings on Trapridge Glacier, Yukon Territory, Canada. *J. Glaciol.*, **14**(70), 79–84.

Gorman, M. R. and A. P. R. Cooper. 1987. A digital radio echo-sounding and navigation recording system. *Ann. Glaciol.*, **9**, 81–84.

Gudmandsen, P. 1969. Airborne radio echo sounding of the Greenland ice sheet. *Geogr. J.*, **135**(4), 548–551.

Gudmandsen, P. E. 1970. Notes on radar sounding of the Greenland ice sheet. *In* Gudmandsen, P. E., *ed. Proceedings of the International Meeting on Radioglaciology, May 1970, Lyngby, Denmark.* Lyngby, Technical University of Denmark. Laboratory of Electromagnetic Theory, 124–135.

Gudmandsen, P. 1975. Layer echoes in polar ice sheets. *J. Glaciol.*, **15**(73), 95–101.

Gudmandsen, P. 1977. Studies of ice by means of radio echo sounding. *In* Peel, R. F., L. F. Curtis and E. C. Barrett, *eds. Remote sensing of the terrestrial environment.* London, etc., Butterworths, 198–211.

Hamran, S. -E. and E. Aarholt. 1993. Glacier study using wavenumber domain synthetic aperture radar. *Radio Sci.*, **28**(4), 559–570.

Hargreaves, N. D. 1977. The polarization of radio signals in the radio echo sounding of ice sheets. *J. Phys. D*, **10**(9), 1285–1304.

Harrison, C. H. 1971. Radio-echo sounding: focusing effects in wavy strata. *Geophys. J. R. Astron. Soc.*, **24**(4), 383–400.

Harrison, C. H. 1973. Radio echo sounding of horizontal layers in ice. *J. Glaciol.*, **12**(66), 383–397.

Hempel, L. and F. Thyssen. 1993. Deep radio echo soundings in the vicinity of

GRIP and GISP2 drill sites, Greenland. *Polarforschung*, **62**(1), 1992, 11–16.
Hodge, S. M., D. L. Wright, J. A. Bradley, R.W. Jacobel, N. Skou and B. Vaughn. 1990. Determination of the surface and bed topography in central Greenland. *J. Glaciol.*, **36**(122), 17–30.
Jacobel, R.W. and S. M. Hodge. 1995. Radar internal layers from the Greenland summit. *Geophys. Res. Lett.*, **22**(5), 587–590.
Jezek, K. 1985. Radar measurements of borehole geometry on the Greenland and Antarctic ice sheets. *Geophysics*, **50**(2), 242–251.
Jezek, K. C., C. R. Bentley and J.W. Clough. 1979. Electromagnetic sounding of bottom crevasses on the Ross Ice Shelf, Antarctica. *J. Glaciol.*, **24**(90), 321–330.
Kotlyakov, V. M. and Yu.Ya. Macheret. 1987. Radio echo-sounding of subpolar glaciers in Svalbard: some problems and results of Soviet studies. *Ann. Glaciol.*, **9**, 151–159.
Krabill, W. B., R. H. Thomas, C. F. Martin, R. N. Swift and E. B. Frederick. 1995a. Accuracy of airborne laser altimetry over the Greenland ice sheet. *Int. J. Remote Sensing*, **16**(7), 1211–1222.
Krabill, W., R. Thomas, K. Jezek, K. Kuivinen and S. Manizade. 1995b. Greenland ice sheet thickness changes measured by laser altimetry. *Geophys. Res. Lett.*, **22**(17), 2341–2344.
Legarsky, J. J., S. P. Gogineni, C. Allen, T. S. Chuah and Y. C. Wong. 1997. *Radar thickness measurements over the northern part of the Greenland ice sheet: 1996 results.* Lawrence, KS, University of Kansas Center for Research Inc. Radar Systems and Remote Sensing Laboratory. (Technical Report 10470-6.)
Macheret, Yu.Ya. and A. B. Zhuravlev. 1982. Radio echo-sounding of Svalbard glaciers. *J. Glaciol.*, **28**(99), 295–314.
Millar, D. H. M. 1981. Radio-echo layering in polar ice sheets and past volcanic activity. *Nature*, **292**(5822), 441–443.
Morgan, V. I. and W. F. Budd. 1975. Radio-echo sounding of the Lambert Glacier basin. *J. Glaciol.*, **15**(73), 103–111.
Musil, G. J. and C. S. M. Doake. 1987. Imaging subglacial topography by a synthetic aperture radar technique. *Ann. Glaciol.*, **9**, 170–175.
Narod, B. B. and G. K. C. Clarke. 1980. Airborne UHF radio echo-sounding of three Yukon glaciers. *J. Glaciol.*, **25**(91), 23–31.
Narod, B. B. and G. K. C. Clarke. 1994. Miniature high-power impulse transmitter for radio-echo sounding. *J. Glaciol.*, **40**(134), 190–194.
Neal, C. S. 1976. Radio-echo power profiling. *J. Glaciol.*, **17**(77), 527–530.
Neal, C. S. 1979. The dynamics of the Ross Ice Shelf revealed by radio echo-sounding. *J. Glaciol.*, **24**(90), 295–307.
Nolan, M., R. J. Motyka, K. Echelmeyer and D. C. Trabant. 1995. Ice-thickness measurements of Taku Glacier, Alaska, U.S.A., and their relevance to its recent behavior. *J. Glaciol.*, **41**(139), 541–553.
Oswald, G. K. A. 1975. Investigation of sub-ice bedrock characteristics by radio-echo sounding. *J. Glaciol.*, **15**(73), 75–87.
Paterson, W. S. B. 1994. *The physics of glaciers. Third edition.* Oxford, etc., Elsevier.
Raju, G., W. Xin and R. K. Moore. 1990. Design, development, field observations, and preliminary results of the coherent Antarctic radar depth sounder (CARDS) of the University of Kansas, U.S.A. *J. Glaciol.*, **36**(123), 247–254.
Rignot, E. 1996. Tidal motion, ice velocity and melt rate of Petermann Gletscher, Greenland, measured from radar interferometry. *J. Glaciol.*, **42**(142), 476–485.
Rinker, J. N. Unpublished. Monocycle radio ice measurements, 1966 Greenland field tests. Hanover, NH, U.S. Army Corps of Engineers. Cold Regions Research and Engineering Laboratory. (Report.)
Rinker, J. N. and S. J. Mock. 1967. Radar ice thickness profiles — northwest Greenland. *CRREL Spec. Rep.* 103.
Robin, G. de Q. 1972. Polar ice sheets: a review. *Polar Rec.*, **16**(100), 5–22.
Robin, G. de Q. 1975a. Radio-echo sounding: glaciological interpretations and applications. *J. Glaciol.*, **15**(73), 49–64.
Robin, G. de Q. 1975b. Velocity of radio waves in ice by means of a bore-hole interferometric technique. *J. Glaciol.*, **15**(73), 151–159.
Sinsheimer, R. L. 1947. Altitude determination. *In* Hall, J. S., *ed. Radar aids to navigation.* New York, etc., McGraw-Hill, 131–142. (MIT Radiation Laboratory Series 2.)
Sivaprasad, K., *ed.* 1978. *Report of radio echo sounding of ice workshop, Durham, New Hampshire.* Durham, NH, University of New Hampshire. Department of Electrical and Computer Engineering.
Strangway, D.W. *and 7 others.* 1974. Radio-frequency interferometry — a new technique for studying glaciers. *J. Glaciol.*, **13**(67), 123–132.
Sverrisson, M., Æ. Jóhannesson and H. Björnsson. 1980. Radio-echo equipment for depth sounding of temperate glaciers. *J. Glaciol.*, **25**(93), 477–486.
Waite, A. H. and S. J. Schmidt. 1961. Gross errors in height indication from pulsed radar altimeters operating over thick ice or snow. *Institute of Radio Engineers International Convention Record*, **5**, 38–53.
Walford, M. E. R. 1964. Radio echo sounding through an ice shelf. *Nature*, **204**(4956), 317–319.
Walford, M. E. R. and M. F. L. Harper. 1981. The detailed study of glacier beds using radio-echo techniques. *Geophys. J. R. Astron. Soc.*, **67**(3), 487–514.
Walford, M. E. R., P. C. Holdorf and R. G. Oakberg. 1977. Phase-sensitive radio-echo sounding at the Devon Island ice cap, Canada. *J. Glaciol.*, **18**(79), 217–229.
Watts, R. D. and A.W. England. 1976. Radio-echo sounding of temperate glaciers: ice properties and sounder design criteria. *J. Glaciol.*, **17**(75), 39–48.
Watts, R. D. and D. L. Wright. 1981. Systems for measuring thickness of temperate and polar ice from the ground or from the air. *J. Glaciol.*, **27**(97), 459–469.
Watts, R. D., A.W. England, R. S. Vickers and M. F. Meier. 1975. Radio-echo sounding on South Cascade Glacier, Washington, using a long-wavelength, mono-pulse source. (Abstract.) *J. Glaciol.*, **15**(73), 459–461.
Weber, J. R. and P. Andrieux. 1970. Radar soundings on the Penny Ice Cap, Baffin Island. *J. Glaciol.*, **9**(55), 49–54.
West, J. C. and K. R. Demarest. 1987. The radiation characteristics of an arbitrary antenna positioned on a polar ice sheet. *Geophysics*, **52**(12), 1689–1696.
Woodruff, A. H.W. and C. S. M. Doake. 1979. Depolarization of radio waves can distinguish between floating and grounded ice sheets. *J. Glaciol.*, **23**(89), 223–232.
Wright, D. L., S. M. Hodge and J. A. Bradley. 1989. Use of a new high-speed digital data acquisition system for airborne ice-sounding. *IEEE Trans. Geosci. Remote Sensing*, **GE-27**(5), 561–567.
Xin, W. 1989. *Data processing system of the coherent Antarctic radar depth sounder.* Lawrence, KS, University of Kansas Center for Research Inc. Radar Systems and Remote Sensing Laboratory. (Technical Report 8070-3.)

MS received 26 November 1997 and accepted in revised form 5 May 1998